

Article

Simulation of Coupled Heat-Mass Transfer in Sea Cucumbers with Heat Pump Drying

Haibo Zhao ¹, Jiaao Dai ² and Kun Wu ^{3,*}

¹ School of Ocean, Yantai University, Yantai 264005, China; zhaohaibo@ytu.edu.cn

² School of Environmental Science and Engineering, Donghua University, Shanghai 201620, China; 1209112@mail.dhu.edu.cn

³ Department of Automobile and Ship Engineering, Yantai Vocational College, Yantai 264670, China

* Correspondence: 20190023@ytvc.edu.cn

Abstract: To study the heat and moisture transfer behavior in sea cucumbers with heat pump convective drying, a multi-physical field coupled model including the velocity field, temperature field, and dilute matter transfer in the porous media of sea cucumbers is built. The heat pump drying experiments verified the results of numerical simulation. The results show that the moisture content on the dry basis of a sea cucumber decreases from the surface to the inside. The sea cucumber's surface temperature increases gradually with drying until it reaches an equilibrium temperature, while the time required decreases with the increase in wind speed. The dry basis moisture content at the center of three different samples decreases from the initial values of 17.29, 13.48, and 7.73 to 3.25, 1.80, and 0.66, respectively. Further, the surface temperatures reached 40 °C, 33 °C, and 30 °C, which are the same as the inlet temperature. The simulated results were within 11% of the experimental ones, showing good consistency for both the dry basis moisture contents and temperatures. This research proves that a coupled heat and mass transfer model based on the porous medium theory can well describe the heat and mass transfer characteristics of sea cucumber with heat pump drying. It is also useful for studies on drying process optimization and quality improvement of aquatic products with heat pump drying.



Citation: Zhao, H.; Dai, J.; Wu, K. Simulation of Coupled Heat-Mass Transfer in Sea Cucumbers with Heat Pump Drying. *Appl. Sci.* **2022**, *12*, 5508. <https://doi.org/10.3390/app12115508>

Academic Editor: Xiaohong Han

Received: 25 April 2022

Accepted: 26 May 2022

Published: 29 May 2022

Publisher's Note: MDPI stays neutral with regard to jurisdictional claims in published maps and institutional affiliations.



Copyright: © 2022 by the authors. Licensee MDPI, Basel, Switzerland. This article is an open access article distributed under the terms and conditions of the Creative Commons Attribution (CC BY) license (<https://creativecommons.org/licenses/by/4.0/>).

Keywords: heat pump drying; heat transfer; mass transfer; dry basis moisture content

1. Introduction

The protein content of a sea cucumber is high, but its sugar content is low, so it has great nutritional and medicinal value. However, because of their seasonal production and easy self-dissolution, sea cucumbers should be processed early in their production cycle to facilitate their transport, storage, and nutritional value retention. Drying is one of the most important methods used to process sea cucumbers.

Duan [1] and Yuan [2] introduced the current methods of drying sea cucumbers by using modern food processing practices. They all mentioned in their research that the drying of seafood should be carried out at a lower temperature. Mu et al. [3] concluded that the heat pump drying speed is faster when the drying air has lower relative humidity, higher velocity, and smaller size. Zheng [4] described the development of heat pump drying technology and its application in drying agricultural by-products. Sun et al. [5] studied the convective drying process and characteristics of sea cucumbers at different temperatures, and the optimum drying temperature was determined to be 45 °C.

In order to further refine the optimal drying process and improve the quality of the dry product, mathematical simulation methods are used for the heat pump drying research [6]. For example, Zhao H B et al. [7] studied the water loss of cabbage seeds by heat pump drying and established four different drying models when the temperature of the dry air and the relative humidity were different. Chen G X et al. [8] established a three-dimensional physical model of a large warehouse to study its heat and moisture

transfer processes of cooling, drying, and ventilation. Wang Y F [9] studied specific drying processes with numerical simulation and experimental verification to explore the effects of pressure, temperature, wind speed, and air humidity on tea drying. Zheng B H et al. [10] established a thermal and mass transfer model of wood to simulate the relationship between temperature and moisture content with drying time. It can be seen that the change in wind speed will also have a great impact on the drying process. Kong N H [11] discussed the effects of drying parameters in-depth, looking at the effects of hot air temperature, initial moisture content, and hot air speed on monomer corn granule drying characteristics and stress. Li W R et al. [12] studied the heat pump drying characteristics of mushrooms. The experimental results showed that the drying temperature of the heat pump suitable for mushroom is 55 °C. B. A. Fu et al. [13] established a mathematical model of intermittent infrared convection. The results showed that the final product quality after batch infrared convective drying was higher than that of convective hot air drying. Daniel I et al. [14] developed a mathematical model of infrared and hot wind combined drying in which the relationship between temperature, shrinkage, and diffusion rate was considered to accurately predict the change in moisture content and temperature distribution in sweet potatoes. C.L. Hii et al. [15] studied a dynamic model of cocoa bean heat pump drying under varied conditions. A shrinkage factor was incorporated into the heat and mass transfer model.

In recent years, with the further study of heat and mass transfer in porous media, a porous media model of materials has been used to analyse the heat and mass transfer characteristics in drying processes. Sabarez et al. [16] described the coupled transfer of momentum, heat, and mass in air and food and predicted the convective drying process of plums. Zhu D G et al. [17] established a two-dimensional mathematical model of heat and mass transfer in the convective drying of food. Yuan et al. [18] built a porous media network model based on an analysis of the parameters of natural porous media and analysed the moisture migration mechanism in the drying process. Chen et al. [19] carried out a numerical simulation of the water migration and three-phase transformation process in porous thermal insulation materials under large temperature differences based on the thermodynamic equilibrium hypothesis and dynamic boundary conditions.

It can be seen from the above literature that temperature and wind speed are two important factors affecting the drying process. As a typical porous medium, sea cucumber contains different components such as liquid water and steam. At present, the heat mass coupling transfer mechanism of sea cucumber under different working conditions is not clear. In this paper, a heat and mass transfer model in a porous medium was established to understand, in depth, the heat-moisture coupled transfer characteristics of sea cucumbers during heat pump drying, which helps to master the convective drying mechanism and optimize the convective drying process of seafood.

2. Materials and Methods

2.1. Experimental Materials

Three groups of experimental materials were selected, and two parallel contrast samples were identified in each group. The body weight of sea cucumber No. 1 was (30 ± 0.5) g, and the radii of length and width were 43 ± 2 mm and 24 ± 2 mm, respectively. The body weight of sea cucumber No. 2 was (18.9 ± 0.5) g, and the radii of length and width were 35 ± 2 mm and 20 ± 2 mm, respectively. The body weight of sea cucumber No. 3 was (17.2 ± 0.5) g, the radii of length and width were 35 ± 2 mm and 18 ± 2 mm, respectively.

2.2. Instruments and Equipment

The measuring instruments included the YH-A6002 electronic balance (Shanghai Yingheng Weighing Equipment Co., Ltd., Shanghai, China, accuracy is ± 0.001 g), PT100 thermal resistances (Xi'an Xiaxi Electronic Technology Co., Ltd., Xi'an, China, accuracy is ± 1 °C), hot wire anemometer (Qingdao Juchuang Environmental Protection Group Co., Ltd., Qingdao, China, accuracy is ± 0.5 m/s), and heat pump drying equipment (Figure 1).

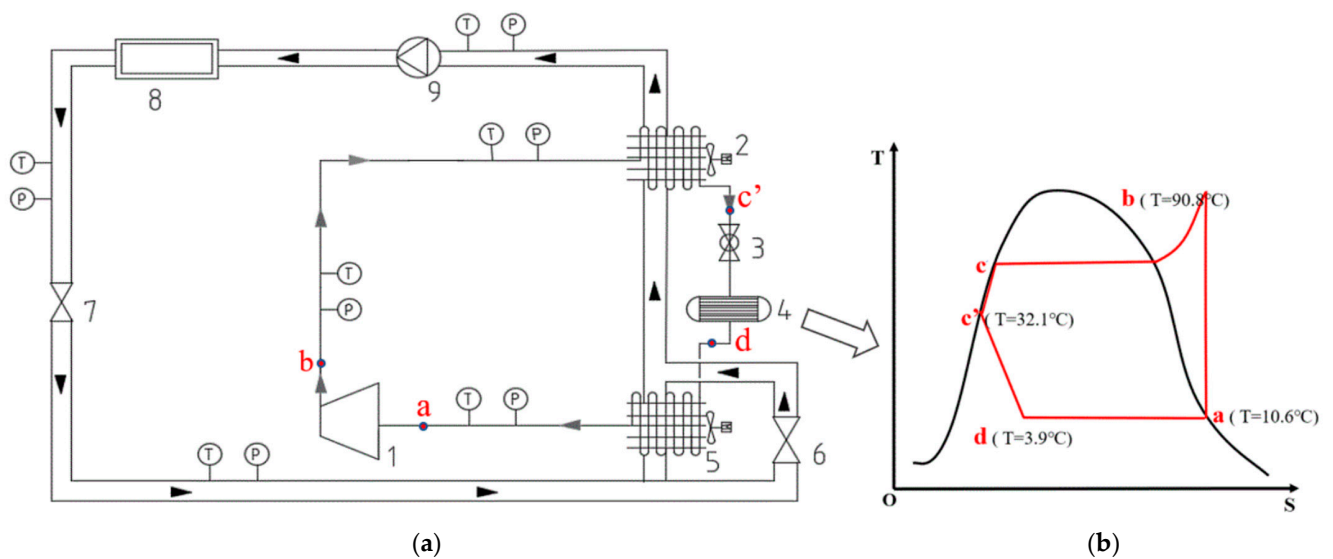


Figure 1. Heat pump dryer (a) schematic diagram and (b) T-S diagram of heat pump. Note: 1—compressor, 2—condenser, 3—throttle valve, 4—receiver, 5—evaporator, 6—first bypass valve, 7—s second bypass valve, 8—drying oven, 9—circulating fan. a—compressor inlet, b—condenser inlet, c—condenser outlet, d—evaporator inlet.

The experimental system consists of a heat pump circuit and a dry air circuit. The heat pump loop includes a compressor (1), condenser (2), throttle valve (3), reservoir (4), evaporator (5), and corresponding connecting pipeline; the dry air loop includes a drying oven (8), circulating fan (9), air flow regulating valve, bypass valve, and other components. The device utilizes a reverse Carnot cycle to recover waste air heat at the outlet of the drying oven to realize cyclic heating. When the refrigerant enters the compressor (1), it is heated and high-pressure gas flows into the condenser (2), heats the dry air and condenses into liquid, enters the throttle valve through the reservoir (4), and becomes a low temperature and low-pressure gas–liquid mixture to flow back to the evaporator (5) to absorb heat. In the drying air circuit, the air enters the condenser (2) to absorb heat and temperature rises, then enters the drying equipment driven by the fan to dry the material, then absorbs the moisture of the material and flows out of the drying equipment. After passing through the airflow regulating valve, the air is divided into two paths, one through the first bypass (6) to the evaporator to dehumidify, the other through the second bypass (7) ventilation regulating valve. The two air paths are mixed and then heated in the condenser to complete the air loop circulation. The side ventilation regulating valve can regulate the temperature and humidity of the dry air.

2.3. Experimental Steps

Before each test, the heat pump's drying temperature was set to 40 °C, 33 °C, and 30 °C (temperature difference ± 1 degrees Celsius). The experiment began after the temperature was stable. The wind speed in the drying equipment was set to 3.3 m/s. The steps were:

- For pretreatment, a fresh sea cucumber was boiled in water for 10 min.
- The boiled sea cucumber was weighed and its initial size was measured.
- The sea cucumber was put into the drying equipment, and the air outlet temperature was set to one of the above temperatures in turn. Two temperature measuring points were arranged on the surface and inside of the sample. After the drying machine was running, the sea cucumber was weighed and measured every 20 min. The length of the test was set at 600 min.
- The above steps were repeated three times, and their average results were analyzed.

2.4. Test Quantity and Calculating Formulas

(1) Dry-base moisture

Dry-base moisture content was determined by the atmospheric drying method specified in the GB/T5009.3-2016 National Food Safety Standard.

$$M_{db} = \frac{m_t - m_g}{m_g} \quad (1)$$

where M_{db} is the moisture content on dry basis, c_w is the water concentration, c_v is the vapor concentration, ϕ is the porosity, and ρ_s is the density of the solid skeleton.

(2) Relative deviation rate

$$E_{MD} = \frac{y_1 - y_2}{y_1} \times 100\% \quad (2)$$

where y_1 is the experimental value and y_2 is the simulated value.

(3) Correlation coefficient

$$R^2 = 1 - \frac{\sum_{i=1}^m \frac{(y_i - \hat{y}_i)^2}{m-j-1}}{\sum_{i=1}^m \frac{(y_i - \bar{y})^2}{m-1}} \times 100\% \quad (3)$$

where y is the fitting value, \hat{y}_i is the corresponding experimental value, m is the number of data, i is the group experiment, and j is the number of constants.

2.5. Physical Model

In order to simplify the model and improve the efficiency of its numerical simulation, the following assumptions are proposed: hot air enters the inlet of the drying equipment and flows through the ellipsoidal material to be dried in the axial direction, the temperature and moisture content of the sea cucumber were uniformly distributed in its initial state, and the effect of porosity change on internal water transfer due to volume shrinkage of the sea cucumber during drying was neglected.

Under the above assumptions, a two-dimensional axisymmetric model of heat pump drying of sea cucumber was established by taking the whole sea cucumber as the test sample and considering its axisymmetric characteristics, as shown in Figure 2.

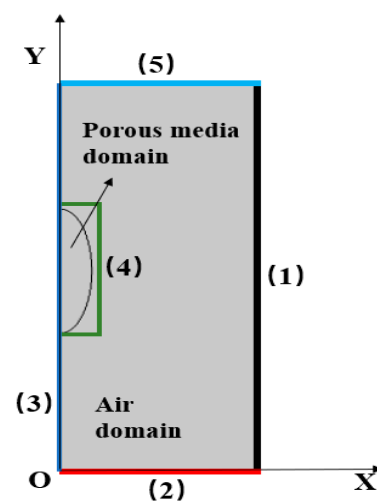


Figure 2. Schematic diagram of two-dimensional axisymmetric model of sea cucumber in drying oven. Note: Figure 2 shows the cross-section view of the desiccating box and the model of the sea cucumber; the middle line is the axis of symmetry, the desiccating box is 24 cm wide, 30 cm high, the long axis of the sea cucumber is 7 cm, and the short axis is 4 cm.

2.6. Governing Equations

The sea cucumber is a heterogeneous porous medium [20]. Its volume component is defined as

$$V = V_s + V_w + V_g \quad (4)$$

The porosity ϕ is described as

$$\phi = \frac{V_w + V_g}{V} \quad (5)$$

where V_s is the solid phase component, V_w is the liquid phase component, V_g is the gas phase component, and ϕ is the porosity.

The water saturation S_w and the air saturation S_g are defined as the volume fractions of water and gas in the pore volume, respectively.

$$S_w = \frac{\Delta V_w}{\Delta V_w + \Delta V_g} = \frac{\Delta V_w}{\phi \Delta V} \quad (6)$$

$$S_g = \frac{\Delta V_g}{\Delta V_w + \Delta V_g} = \frac{\Delta V_g}{\phi \Delta V} \quad (7)$$

The water concentration of the porous medium is defined as [21]

$$c_w = S_w \times \phi \times \rho_w / M_w \quad (8)$$

where ϕ is the porosity, ρ_w is the density of the fluid, S_w is the water saturation, and M_w is the molecular weight.

The vapor concentration at ambient temperature is defined as [21]

$$c_v = 610.7 \times 10^6 (7.5 \times (T - 273.1) / (T - 35.8)) / R / T \quad (9)$$

where T is the air temperature, R is the gas constant, and c_v is the vapor concentration.

The evaporation source phase R_{evap} is defined as [21]

$$R_{evap} = K_{evap} \frac{M_w}{RT} (c_{v,sat} - c_v) S_g \phi \quad (10)$$

where K_{evap} is the evaporation rate constant, M_w is the molecular weight, c_v is the vapor concentration, and $c_{v,sat}$ is the saturated vapor concentration.

The dry basis moisture content of sea cucumber is defined as [21]

$$M_{db} = \frac{c_w + c_v}{(1 - \phi) \rho_s} \quad (11)$$

where M_{db} is the moisture content on dry basis, c_w is the water concentration, c_v is the vapor concentration, ϕ is the porosity, and ρ_s is the density of the solid skeleton.

The momentum equation in the drying oven is

$$\rho_g \frac{\partial u}{\partial t} + \rho_g (u \cdot \nabla) u = -\nabla p + \nabla \cdot \left[(\mu_g + \mu_T) (\nabla u + (\nabla u)^T) - \frac{2}{3} (\mu_g + \mu_T) \nabla \cdot u \right] \quad (12)$$

The momentum equation in the porous medium region is

$$\begin{aligned} \frac{\rho_g}{S_g \phi} \frac{\partial u}{\partial t} + \frac{\rho_g}{S_g \phi} (u \cdot \nabla) u \frac{1}{\phi S_g} = & -\nabla p + \nabla \cdot \left[\frac{\mu_g}{\phi S_g} (\nabla u + (\nabla u)^T) \right. \\ & \left. - \frac{2}{3} \frac{\mu_g}{\phi S_g} (\nabla \cdot u) \right] - \left(\mu_g k_{gr}^{-1} + \frac{1}{2} \rho_g F |u| \right) u \end{aligned} \quad (13)$$

where ρ_g is the density, μ_g is the dynamic viscosity of air, μ_T is the turbulent viscosity, t is the time, F is the relaxation function, and ϕ is the porosity.

The mass transfer of vapor occurs in the drying oven and porous media, whereas that of water occurs only in the porous media. The mass equations for the drying oven and porous media are described as follows:

Mass equations for vapor and water in the porous media:

$$\frac{\partial c_v}{\partial t} + \nabla \cdot n_v = R_{\text{evap}} \quad (14)$$

$$\frac{\partial c_w}{\partial t} + \nabla \cdot n_w = -R_{\text{evap}} \quad (15)$$

Mass equation for vapor in the drying oven:

$$\frac{\partial c_v}{\partial t} + \nabla \cdot n_v = 0 \quad (16)$$

where n_v and n_w are the mass fluxes of vapor and water, respectively. c_w is the water concentration, and c_v is the vapor concentration.

The mass flux of vapor in the porous media can be described as [22]

$$n_v = uc_v - D_{va} \nabla c_v. \quad (17)$$

The mass flux of water in the porous media can be described as [22]

$$n_w = uc_w - D_{cap} \nabla c_w. \quad (18)$$

where u is the superficial velocity of the fluid, D_{va} is the vapor diffusion coefficient, and D_{cap} is capillary diffusion coefficient.

The heat transfer equation in the drying oven is

$$\frac{\partial (\rho_a c_{p,g} T)}{\partial t} + \nabla \cdot (\rho_a c_{p,g} u T) = \nabla \cdot (\lambda_g \nabla T) \quad (19)$$

The heat transfer equation in the porous medium is

$$\frac{\partial ((\rho c_p)_{\text{eff}} T)}{\partial t} + \nabla \cdot (J_s c_{p,s} T + J_l c_{p,w} T + J_a c_{p,g} T) = \nabla \cdot (\lambda_{\text{eff}} \nabla T) - R_{\text{evap}} h_{\text{evap}} \quad (20)$$

The effective thermophysical parameters are defined as

$$\lambda_{\text{eff}} = (1 - \phi) \lambda_s + S_w \phi \lambda_w + \phi \lambda_g (1 - S_w) \quad (21)$$

$$(\rho c_p)_{\text{eff}} = \rho_s c_{p,s} (1 - \phi) + \rho_l c_{p,l} \phi S_w + \rho_a c_{p,a} \phi (1 - S_w) \quad (22)$$

where ρ_{eff} , $c_{p,\text{eff}}$, and λ_{eff} are the effective density, specific heat capacity, and thermal conductivity, respectively, calculated by weighting each component, liquid water and air, respectively. h_{evap} is the latent heat of evaporation, S_w is the water saturation, and T is the temperature.

2.7. Boundary Condition

For a better understanding, the boundary conditions of the above physical model are shown in Figure 2. Each boundary condition is described as follows: labels (1) and (3) represent the outer wall and rotation boundary of the drying oven, respectively. Label (2) represents the inlet of the drying oven, where the air velocity and temperature are constant, and (4) represents the contact surface between the sea cucumber and hot air. There was no water seepage on the surface during the process; hence, the normal gradient of the water concentration was zero. Label (5) is the outlet of the drying oven; hence, the normal gradient of all physical variables was zero. The boundary conditions of the drying oven are listed in Table 1, respectively.

Table 1. Boundary conditions.

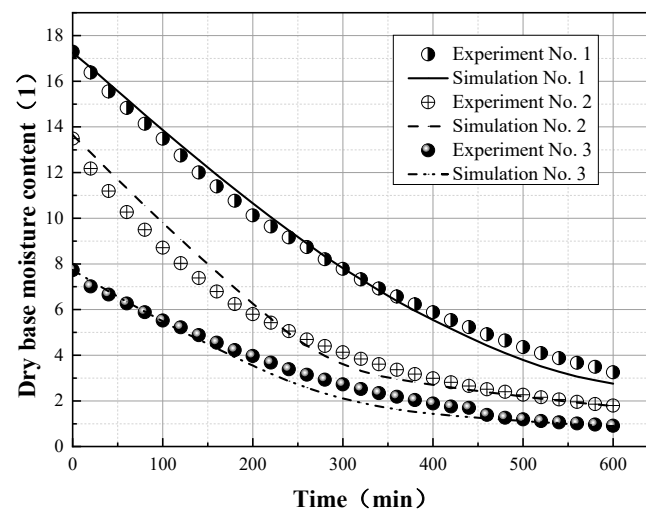
	(1)	(2)	(3)	(4)	(5)
Velocity	0	u_{in}	0	-	$(\nabla u) \cdot n = 0$
Temperature	$(\nabla T) \cdot n = 0$	T_{in}	$(\nabla T) \cdot n = 0$	-	$(\nabla T) \cdot n = 0$
Mass concentration of vapor	$(\nabla c_v) \cdot n = 0$	$c_v(RH)$	$(\nabla c_v) \cdot n = 0$	-	$(\nabla c_v) \cdot n = 0$
Mass concentration of water	-	-	-	$(\nabla c) \cdot n = 0$	-

3. Results and Discussions

3.1. Analysis of Temperature and Dry Basis Moisture Content Changes

Based on the above model, combined with the experimental boundary conditions, the inlet speed of the drying oven is 3.3 m/s, the inlet temperatures are 30 °C, 33 °C, and 40 °C, and the inlet pressure is 101,325 Pa.

Under different drying inlet temperature conditions, the simulated dry-base water contents of samples No. 1–3 were compared with experimental data, as shown in Figure 3.

**Figure 3.** Dry-base moisture of sea cucumbers in simulation and experiments.

From Figure 3, it can be seen that both the simulated and experimental values of dry-base water content decrease exponentially.

The overall comparison shows that the experimental values of dry-base water content in the initial stage are lower than the simulated values, basically coincide with the simulated values in the middle stage, and, in the later stage, are slightly higher than the experimental values. The trends of simulated and experimental dry-base water contents are virtually the same. The correlation coefficients were 0.969, 0.975, and 0.943, respectively. Specifically, the difference between simulated and experimental values of sea cucumber No. 1 was the largest at 60 min, with a relative deviation rate of 5.2% and a numerical value of 52%. At 80 min for sea cucumber No.2, the maximum difference between the simulated and experimental values of water content in the dry basis appeared, and the relative deviation rate was 11%. The maximum difference between the simulated and experimental values of the dry-base moisture content of sea cucumber No. 3 appeared at 120 min, with a difference of 15% and a relative deviation rate of 2.7%.

Temperature measuring points were arranged on the middle of the sea cucumbers' surfaces. The experimental and simulated temperatures seen at the measuring points are shown in Figure 4.

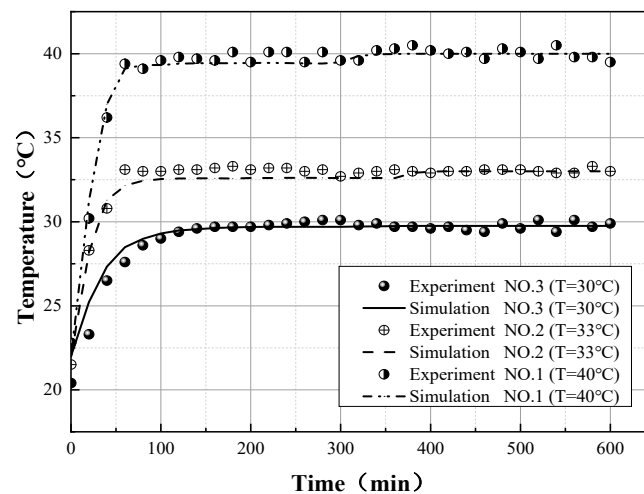


Figure 4. Variations in the surface temperature in sea cucumbers with time and drying temperatures.

It can be seen from Figure 4 that at varying inlet temperatures, the temperatures at the measuring points in the simulation and experimental values gradually increase and, finally, tend to be stable. According to the theory of pervaporation front, the water evaporation process occurs on the surface, and the evaporation from this thin layer changes the surface temperature of the sea cucumber. In the initial stage, the experimental heating rate is higher than that of the simulation, the maximum temperature difference between them is 3 °C, and the experimental and simulation temperatures are both near the stable inlet temperature in the later stage. The correlation coefficients between the experimental and simulation temperatures of three samples are 0.989, 0.986, and 0.971, respectively.

3.2. Effect of Wind Speed on Heat and Mass Transfer Process

Taking the No. 3 sea cucumber as an example, the heat and mass parameters of sea cucumbers during heat pump drying were analyzed by changing the inlet air velocity of the model to 5 m/s, 4 m/s, 3 m/s, 2 m/s, and 1 m/s. The dry-base moisture parameters during heat pump drying were obtained, as shown in Figure 5.

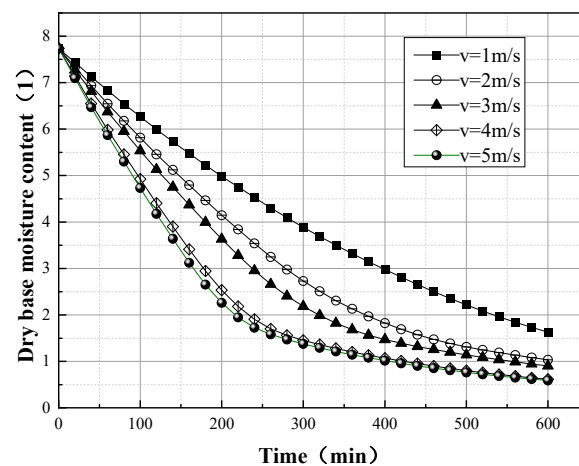


Figure 5. Effect of hot air rate on the dry-base moisture content of sea cucumber.

From Figure 5, we can see that with an increase in inlet air velocity, the rate of water reduction will accelerate. This shows that the drying air velocity is an important parameter in the drying process. A high wind speed can quickly eradicate the moisture content of the material in its initial drying stage, thus accelerating the drying process. When the wind speed is low, the drying time becomes longer. It can be seen from the figure that when the wind speed is 4 m/s, the moisture content of the dry-base decreases to 100% after 400 min;

when the wind speed is 2 m/s, drying needs to proceed to 600 min before the dry-base moisture content reaches that value. As the wind speed is increased, it is seen that there is little difference in the drying rate when the wind speed reaches 4 m/s and 5 m/s. Therefore, it can be concluded that 4 m/s is an economical wind speed for the model.

A plot of the temperature change at the surface point of the sea cucumber's material in the model for different wind speeds is shown in Figure 6.

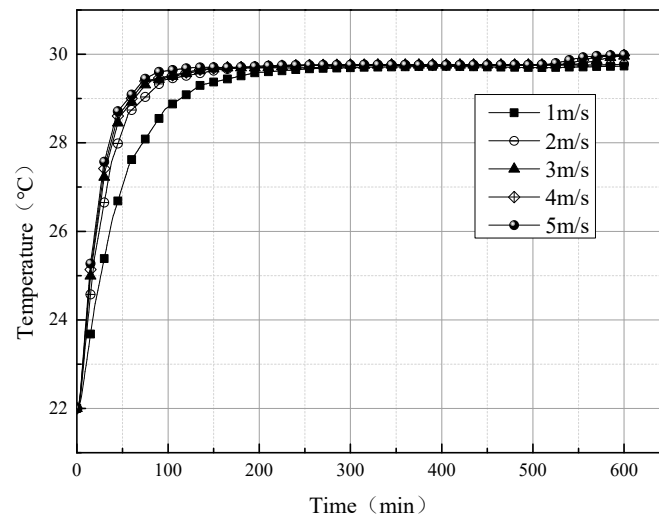


Figure 6. Effect of hot air rate on the surface temperature of sea cucumbers.

It can be seen from Figure 6 that for different inlet wind speeds, the temperature of the material at this measurement point increases rapidly, then slowly rises to the trend of the inlet temperature. Moreover, the higher the hot air speed is, the shorter the time required for the sea cucumber's temperature to reach the inlet temperature. For example, when the hot air rate is 5 m/s, the material temperature reaches a stable value at 100 min; when the hot air rate is 1 m/s, the material surface takes 250 min to reach a stable temperature. The final temperature for 5 m/s is 0.2 °C higher than it is for 1 m/s. There is little difference between the temperature plots of 4 m/s and 5 m/s. It can be seen from the analysis of the simulation results that the material temperature rises rapidly after the start of drying; this is because there is a large temperature difference between the material and the drying medium, and the material temperature is lower than the medium temperature, so there is convective heat transfer from the drying medium to the material. The material temperature rises with the drying process, the moisture inside the material evaporates and absorbs heat, and the material temperature rises slowly. After 600 min, the free water inside the material has evaporated completely, and the surface temperature of the material gradually approaches the inlet temperature of the drying oven.

3.3. Internal Heat and Mass Transfer Law

Taking sea cucumber No. 3 as an example, the variation in dry air velocity, dry-base moisture content, temperature, and concentration in the drying chamber and in the sea cucumber were analyzed for a drying time of 150 min, as shown in Figure 7. As the drying air flows in the chamber, the flow field in the drying chamber changes according to the cross-section area as it flows through the sea cucumber's surface, so the maximum flow rate appears on both sides of the windward end of the drying material. The air velocity distribution affects water evaporation on the sea cucumber's surface and leads to a change in its water content. For example, at 150 min and a velocity of 3.3 m/s in the model, the dry-base moisture content changes to 4.20, and the concentration is 25,000 mol/m³ at the upwind. At the downwind of the sea cucumber, the dry-base moisture content is 4.65, and the concentration is 27,500 mol/m³. The difference in the dry-base moisture content and internal concentration between the two positions is 50% and 2500 mol/m³, respectively.

The difference in the dry-base moisture content increases continuously with drying. At the same time, the air velocity distribution affects temperatures in the materials. The temperature on the windward end is higher than the windward end, which also affects the moisture uniformity in the material during the drying process.

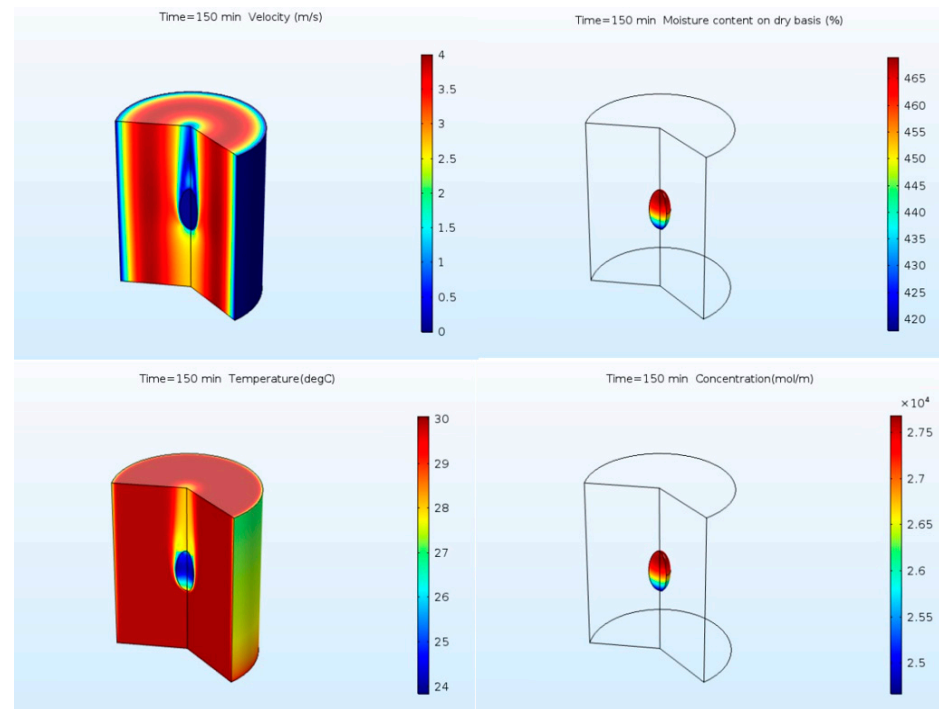


Figure 7. Variation in velocity, dry base moisture content, temperature, and concentration in the drying chamber.

4. Conclusions

In this paper, a mathematical model of the mass transfer and heat transfer characteristics of sea cucumbers is established based on their physical changes during convective drying. The sea cucumbers' transient temperature field and moisture concentration field while drying were simulated, and their dry-base moisture contents, calculated by the Comsol Multiphysics software, were compared to experimental results. The results were as follows:

According to the simulation results, the water content of the sea cucumbers decreases from the surface to the interior, and the temperature decreases from the oven inlet to its outlet during the drying process. In the simulation results, the moisture content at the center points of three different samples decreased from the initial values of 17.29, 13.48, and 7.73 to 3.25, 1.80, and 0.66, respectively. The temperatures reached 40 °C, 33 °C, and 30 °C, which were the same as the inlet temperatures. As drying time increases, the temperature inside the material increases gradually until it reaches an equilibrium temperature. The time to reach the equilibrium temperature decreases with increased inlet wind speed.

For varied inlet temperatures, the change in sample water content simulation results and the experimental results are in good agreement, proving that the model can be used to study sea cucumber drying. The simulated moisture content is slightly lower than the experimental value in the early stage of drying and slightly higher in the later stage, which may be due to a reduced evaporation rate caused by the sea cucumber's size shrinkage and porosity change. The shrinkage model can be considered in the next study to make the simulation results more accurate.

In the drying process, the moisture concentration changes faster in the windward end than in the wind end, which indicates that the single wind direction design of the drying oven in the experiment cannot meet the requirement for uniform distribution of moisture in the drying material. For drying large quantities of product in a large-scale commercial

system, a reversible axial flow fan could reverse the airflow direction periodically to effectively shorten the drying time and ensure uniform drying.

Author Contributions: Conceptualization, H.Z.; methodology, H.Z.; software, H.Z. and J.D.; validation, K.W.; writing—original draft preparation, H.Z. and J.D.; writing—review and editing, K.W.; funding acquisition, H.Z. All authors have read and agreed to the published version of the manuscript.

Funding: This research was funded by the Yantai Science and Technology Plan Project, grant number 2020XDRH097.

Institutional Review Board Statement: Not applicable.

Informed Consent Statement: Not applicable.

Data Availability Statement: Not applicable.

Conflicts of Interest: The authors declare no conflict of interest.

Nomenclature

C	Molar concentration, mol/m ³
C_ϵ	Model constants
c_p	Heat capacity, J/(kg·K)
c	Mass concentration, kg/m ³
$c_{v,sat}$	Saturated vapor concentration, kg/m ³
D	Mass diffusivity, m ² /s
D_{cap}	Capillary diffusion coefficient, m ² /s
D_{va}	Vapor diffusion coefficient, m ² /s
F	Relaxation function
h_{evap}	Latent heat, J/kg
n	Mass flux, kg/(m ² ·s)
K_{evap}	Evaporation rate constant, 1/s
M	Molecular weight, kg/mol
M_{db}	Moisture content on dry basis, 1
P	Pressure, pa
R	Gas constant, kJ/kmol K
R_{evap}	Evaporation rate, kg/(m ³ ·s)
S	Saturation
t	Time, s
T	Temperature, K
T_{in}	Inlet temperature, K
u	Velocity, m/s
u_{in}	Inlet velocity, m/s
	Greek symbols
λ	Thermal conductivity, W/(m·K)
μ	Dynamic viscosity, Pa·s
μ_T	Turbulent dynamic viscosity, Pa·s
ν	Kinematic viscosity, kg/(m·s)
ρ	Density, kg/m ³
ϕ	Porosity
	Subscripts
a	Air
db	Dry basis
eff	Effective
g	Gas
i	Initial
l	Liquid
s	Solid
v	Vapor
sat	Saturated
w	Water

References

1. Duan, X.; Wang, H.; Ren, G.Y.; Zhu, K.R. Drying technology of sea cucumber and its research progress. *Food Ind. Sci. Technol.* **2012**, *33*, 427–431.
2. Yuan, D.L.; Shao, M.; Cai, Z.P. Advances in drying technology of sea cucumber. *Dry. Technol. Equip.* **2015**, *13*, 1–9.
3. Mu, G.; Zhang, G.C.; Shao, L. Preliminary study on heat pump drying of sea cucumber. *Fish. Mod.* **2007**, 47–50. Available online: <https://xueshu.baidu.com/usercenter/paper/show?paperid=fc2eb46e342aac83c0d1cd30f72902dc> (accessed on 20 April 2022).
4. Zheng, C.M. Application of heat pump in drying agricultural by-products. *Agric. Mach. Food Mach.* **1997**, 26–28. [CrossRef]
5. Sun, Y.; Xue, C.H.; Qi, X.M.; Li, Z.J.; Sheng, W.J. Study on the optimum convective drying temperature of sea cucumber. *J. Agric. Eng.* **2007**, *23*, 205–209.
6. Xu, X.M.; Lin, D.H.; Chen, L.; Wang, Y.; Qu, L.B. Optimization of drying process parameters of fresh noodles based on ANSYS numerical simulation. *Chin. J. Grain Oil* **2008**, *33*, 87–93.
7. Zhao, H.B.; Yang, Z.; Dai, J.A.; Qiao, L.M.; Zhang, L.L. Study on Dynamic Model of Chinese Cabbage Seed Heat Pump Drying Process. *J. Agric. Mach.* **2011**, *43*, 118–123.
8. Chen, G.X.; Zhang, H.W.; Wang, H.T.; Liu, C.S.; Yi, J. Study on coupled heat and moisture transfer of grain stack during cooling and ventilation of bunker based on COMSOL. *China J. Cereals Oil* **2018**, *33*, 79–85.
9. Wang, Y.F. Study on the Micro-Level Water Loss Mechanism of Tea Drying Process. Master's Thesis, Zhejiang University of Technology, Hangzhou, China, 2016.
10. Zheng, B.H.; Zhen, W.; Qu, L.; Qian, J.; Yi, S. Modeling and simulation of heat-mass transfer and its application in wood thermal modification. *Results Phys.* **2019**, *13*, 102–203.
11. Kong, N.H. A Simulation Study of Hot Air Drying of Corn Granules Based on Solid Model. Master's Thesis, Northeast University, Shenyang, China, 2013.
12. Li, W.R.; Ren, A.Q.; Chen, G.B.; Xiang, W. Study and simulation of dried apricot mushroom heat pump. *Zhejiang Agric. Sci.* **2016**, *57*, 1128–1130.
13. Fu, B.A.; Chen, M.Q.; Song, J.J. Investigation on the microwave drying kinetics and pumping phenomenon of lignite spheres. *Appl. Therm. Eng.* **2017**, *124*, 371–380. [CrossRef]
14. Onwude, D.I.; Hashim, N.; Abdan, K.; Janius, R.; Chen, G.; Kumar, C. Modelling of coupled heat and mass transfer for combined infrared and hot-air drying of sweet potato. *J. Food Eng.* **2018**, *228*, 12–24. [CrossRef]
15. Hii, C.L.; Law, C.L.; Law, M.C. Simulation of heat and mass transfer of cocoa beans under stepwise drying conditions in a heat pump dryer. *Appl. Therm. Eng.* **2013**, *54*, 264–271. [CrossRef]
16. Sabarez, H.T. Computational modelling of the transport-phenomena occurring during convective drying of prunes. *J. Food Eng.* **2012**, *111*, 279–288. [CrossRef]
17. Zhu, D.G.; Chen, J.R.; Liu, X.X. Numerical simulation of coupled heat and mass transfer in food convection drying. *Agric. Mech. Res.* **2011**, *33*, 49–52.
18. Yuan, Y.J.; Yang, B.B.; Liu, X.D. Modeling and Simulation of pore network with constant temperature and slow drying in porous media. *J. Agric. Mach.* **2007**, *70*, 62–66.
19. Chen, L.; Wang, S.G.; Zhang, T.F.; Jia, Z.G.; Fang, T.Y. Numerical simulation of drying process of porous materials under large temperature difference. *J. Dalian Univ. Technol.* **2018**, *58*, 221–228.
20. Liu, W.; Fan, A.W. *Theory and Application of Heat and Mass Transfer in Porous Media*, 1st ed.; Science Press: Beijing, China, 2006.
21. Datta, A.K. Porous media approaches to studying simultaneous heat and mass transfer in food processes. II: Property data and representative results. *J. Food Eng.* **2007**, *80*, 96–110. [CrossRef]
22. Datta, A.K. Porous media approaches to studying simultaneous heat and mass transfer in food processes. I: Problem formulations. *J. Food Eng.* **2007**, *80*, 80–95. [CrossRef]